Supporting Information for

The impact of Sahara dust aerosols on the three-dimensional structure of precipitation systems with different sizes in spring

Contents of this file

Text S1 describes how to calculate the partial correlations.

Text S2 describes how to calculate the wind speed at 10 m (10mWS), vertical wind shear (VWS) between 850 hPa (~1.5 km) and 500 hPa (~5.5 km), lower tropospheric stability (LTS), relative humidities at low-level (RHlow) and at mid-level (RHmid).

Table S1 shows the proportion (%) of PSs consistent with this study (3 days and 3 grids) after classification using different dust condition estimates by selecting different numbers of days, as well as numbers of grids extending outwards.

Figure S1 shows the average CAPE distribution of different conditions.

Figure S2 shows the mean vertical profiles of median rain rate for total, convective and stratiform precipitation of small-sized PSs with different CAPE values under clean and dusty conditions.

Figure S3 shows the vertical profiles of 10th, 50th, and 90th percentiles of PS maximum radar reflectivity for total, convective and stratiform precipitation of small-sized PSs with different CAPE values under clean and dusty conditions.

Text S1

Calculation of partial correlations

The Pearson correlation (Pearson, 1896) is used to access the strength of associations between AOD and PSs characteristics. The partial correlation is applied to measure the linear dependence between them where the influence from other predictors (i.e., meteorological factors in this case) is removed (Han et al., 2022; Jiang et al., 2018; Zhao et al., 2018). The partial correlation between two variables X1 and X2 eliminating the effects of Y (a vector of parameters) is:

$$\rho_{12\cdot Y} = \frac{\sigma_{12\cdot Y}}{\sqrt{\sigma_{11\cdot Y}\,\sigma_{22\cdot Y}}} \quad (1)$$

where $\sigma_{12\cdot Y}$ is the conditional covariance between X1 and X2, eliminating the effects of Y; $\sigma_{11\cdot Y}$ and $\sigma_{22\cdot Y}$ are the conditional variances of X1 and X2 respectively, eliminating the effects of Y (Baba et al., 2004)

Text S2

Calculation of wind speed at 10 m (10mWS), vertical wind shear (VWS) between 850 hPa (~1.5 km) and 500 hPa (~5.5 km), lower tropospheric stability (LTS), relative humidities at low-level (RHlow) and at mid-level (RHmid)

The wind speed at 10 m is calculated with:

$$10\mathrm{mWS} = \sqrt{{u_{10m}}^2 + {v_{10m}}^2} \quad (2)$$

where u_{10m} and v_{10m} represent U and V components of wind at 10 m.

Vertical wind shear between 850 hPa (~1.5 km) and 500 hPa (~ 5.5 km) is calculated using:

$$\mathrm{VWS} = \left(\sqrt{(u_{500} - u_{850})^2 + (v_{500} - v_{850})^2}\right)/(5500 - 1500) \quad (3)$$

where u_{500} and v_{500} represent U-component and V-component of wind speed at 500 hPa respectively, and u_{850} and v_{850} represent U-component and V-component of wind speed at 850 hPa respectively (Guo et al., 2016; Guo et al., 2018).

LTS is widely used to represent low-level atmospheric stability (Guo et al., 2017; Klein and Hartmann, 1993; Yang et al., 2021)， and is calculated using:

$$\mathrm{LTS} = \theta_{700} - \theta_{1000} \quad (4)$$

where θ_{700} and θ_{1000} represent potential temperature at 700hPa and 1000hPa respectively.

The potential temperature is calculated using:

$$\theta_P = T \times \left(\frac{1000}{P}\right)^{R/C_p} \quad (5)$$

where T represents the temperature at the pressure layer P, R is universal gas constant for dry air, and C_p is the specific heat capacity at constant pressure. $R/C_p = 0.286$.

The relative humidities at low-level (1000-850 hPa) and mid-level (700–400 hPa) are averaged as the indicators of water vapor situation at different altitudes (Liu et al., 2017), referred to as RHlow and RHmid, respectively.

Table S1 The proportion (%) of PSs consistent with this study (3 days and 3 grids) after classification using different dust condition estimates by selecting different numbers of days, as well as numbers of grids extending outwards.

GRID \ DAY	1	2	3	4	5
1	75.7	82.7	85.1	84.9	83.0
2	77.8	89.3	93.0	89.9	88.4
3	82.0	90.9	100.0	91.3	89.3
4	82.1	88.8	93.8	90.3	87.4
5	79.1	86.9	89.1	86.8	84.0

Figure S1 The average CAPE distribution of different conditions: (a) multi-year average CAPE, (b) background CAPE corresponding to clean PSs, (c) background CAPE corresponding to dusty PSs, (d) differences of CAPE between two conditions (dusty-clean).

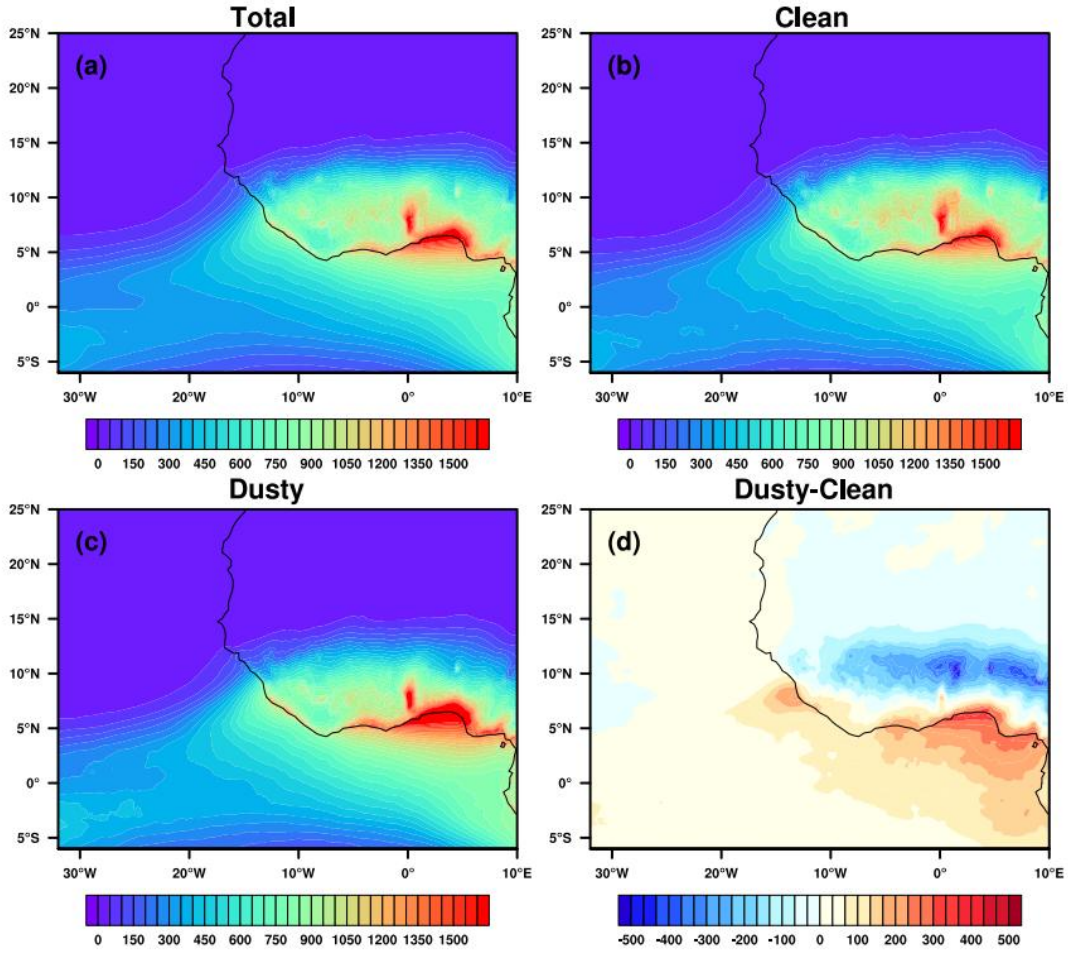

Figure S2 The mean vertical profiles of median rain rate for total (upper row), convective (middle row) and stratiform (bottom row) precipitation of small-sized PSs with different CAPE values under clean and dusty conditions. The black dot on the red line indicates that the difference between clean and dusty conditions is statistically significant at the 95% confidence level using a Student's t-test. The horizontal dashed lines show the freezing level with values labeled.

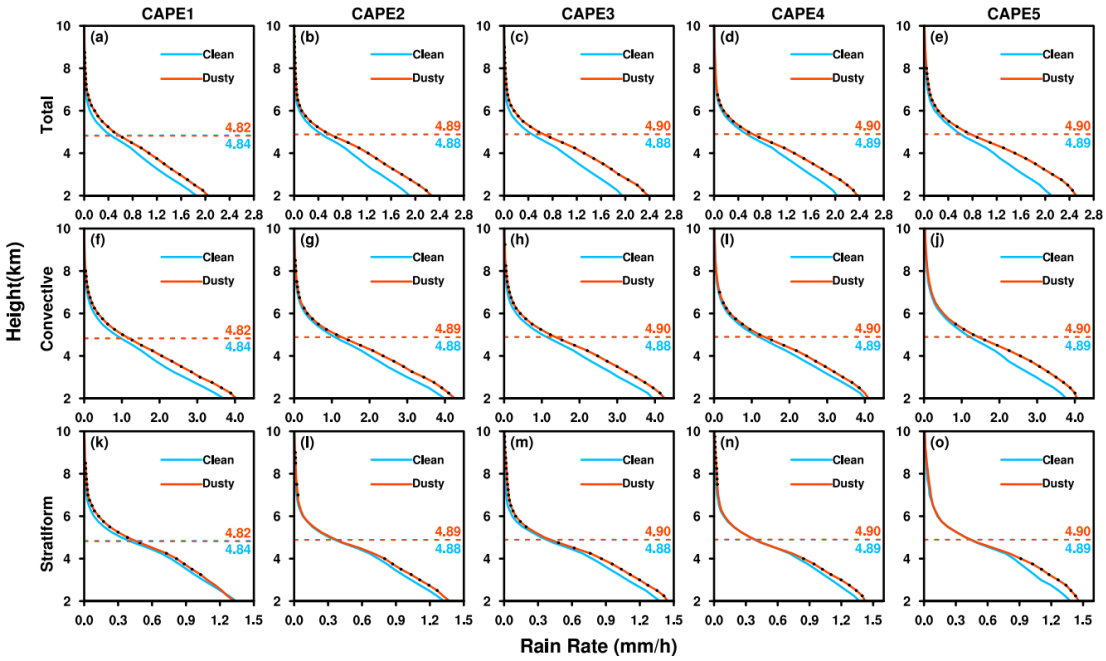

Figure S3 Vertical profiles of 10th, 50th, and 90th percentiles of PS maximum radar reflectivity for total (upper row), convective (middle row) and stratiform (bottom row) precipitation of small-sized PSs with different CAPE values under clean and dusty conditions. The horizontal dashed lines show the freezing level with values labeled.

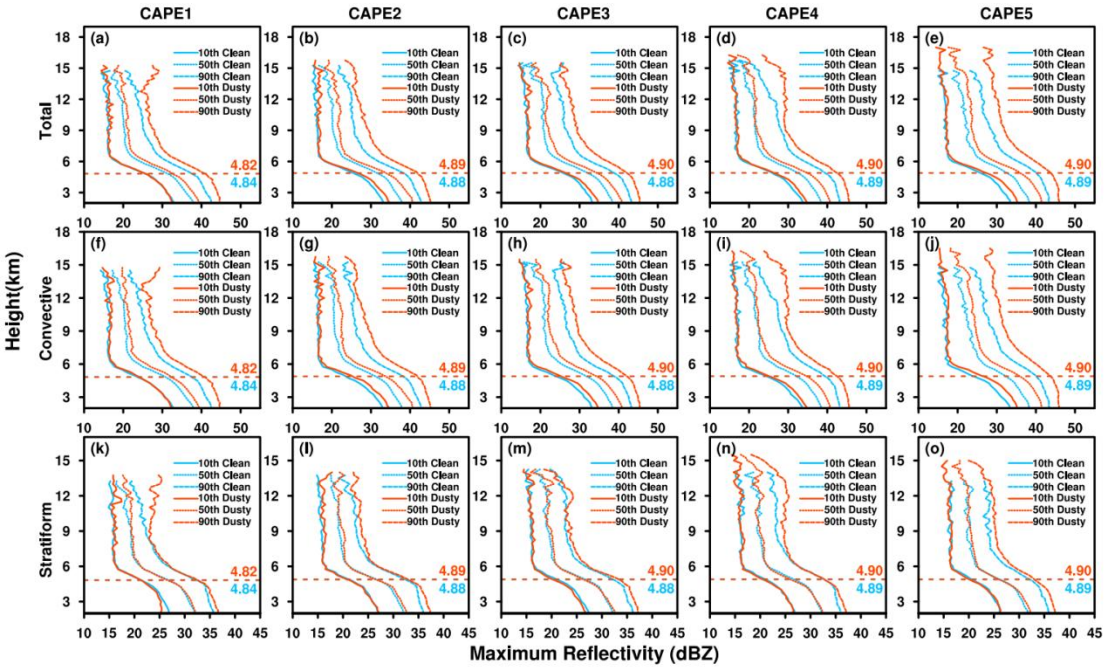

Guo, J., Su, T., Li, Z., Miao, Y., Li, J., Liu, H., Xu, H., Cribb, M., and Zhai, P.: Declining frequency of summertime local-scale precipitation over eastern China from 1970 to 2010 and its potential link to aerosols, Geophysical Research Letters, 44, 5700-5708, 10.1002/2017gl073533, 2017.

Guo, J., Deng, M., Lee, S. S., Wang, F., Li, Z., Zhai, P., Liu, H., Lv, W., Yao, W., and Li, X.: Delaying precipitation and lightning by air pollution over the Pearl River Delta. Part I: Observational analyses, Journal of Geophysical Research: Atmospheres, 121, 6472-6488, 10.1002/2015jd023257, 2016.

Guo, J., Liu, H., Li, Z., Rosenfeld, D., Jiang, M., Xu, W., Jiang, J. H., He, J., Chen, D., Min, M., and Zhai, P.: Aerosol-induced changes in the vertical structure of precipitation: a perspective of TRMM precipitation radar, Atmospheric Chemistry and Physics, 18, 13329-13343, 10.5194/acp-18-13329-2018, 2018.

Han, X., Zhao, B., Lin, Y., Chen, Q., Shi, H., Jiang, Z., Fan, X., Wang, J., Liou, K. N., and Gu, Y.: Type-Dependent Impact of Aerosols on Precipitation Associated With Deep Convective Cloud Over East Asia, Journal of Geophysical Research: Atmospheres, 127, 10.1029/2021jd036127, 2022.

Jiang, J. H., Su, H., Huang, L., Wang, Y., Massie, S., Zhao, B., Omar, A., and Wang, Z.: Contrasting effects on deep convective clouds by different types of aerosols, Nat Commun, 9, 3874, 10.1038/s41467-018-06280-4, 2018.

Klein, S. A. and Hartmann, D. L.: THE SEASONAL CYCLE OF LOW STRATIFORM CLOUDS, Journal of Climate, 6, 1587-1606, 10.1175/1520-0442(1993)006<1587:Tscols>2.0.Co;2, 1993.

Liu, C., Chen, B., and Mapes, B. E.: Relationships between Large Precipitating Systems and Atmospheric Factors at a Grid Scale, Journal of the Atmospheric Sciences, 74, 531-552, 10.1175/jas-d-16-0049.1, 2017.

Pearson, K.: Mathematical Contributions to the Theory of Evolution. III. Regression, Heredity, and Panmixia, Philosophical Transactions of the Royal Society of London Series A, 187, 253-318, 10.1098/rsta.1896.0007, 1896.

Yang, Y., Zhao, C., Wang, Y., Zhao, X., Sun, W., Yang, J., Ma, Z., and Fan, H.: Multi-Source Data Based Investigation of Aerosol-Cloud Interaction Over the North China Plain and North of the Yangtze Plain, Journal of Geophysical Research: Atmospheres, 126, 10.1029/2021jd035609, 2021.

Zhao, B., Gu, Y., Liou, K. N., Wang, Y., Liu, X., Huang, L., Jiang, J. H., and Su, H.: Type-Dependent Responses of Ice Cloud Properties to Aerosols From Satellite Retrievals, Geophys Res Lett, 45, 3297-3306, 10.1002/2018GL077261, 2018.